Seamless Transition of Interior Permanent Magnet Synchronous Motor Base on Back Electromotive Force Observer

Nguyễn Đức Quang[1,2], Cù Đức Tài Lương[1], Giáp Văn Nam[1*], Vũ Hoàng Phương[1*]

[1]Đại học Bách khoa Hà Nội, [2]Trường Đại học Công nghiệp Hà Nội
[*] Corresponding author E-mail: phuong.vuhoang@hust.edu.vn; nam.giapvan@hust.edu.vn

Abstract

Electric motors are important in many fields such as industrial automation, electric vehicles, and other advanced devices. The increasing popularity of applications related to electric motors, especially in the transition from depleting non-reusable energy sources to electric power, has raised a demand for research and development in motor control. In operation mode, the sensor fault can affect the safety of users. Therefore, this paper presents an operation that considers two modes. Firstly, the motor is controlled using a field-oriented control strategy with an absolute encoder. Second, assuming a sensor fault occurs during operation, fault detection and switching commands are used to change the signal source. The key contribution of this work lies in the design of an effective observer and fault detection algorithm, which accurately estimates the motor's state variables and identifies sensor faults in real-time. By seamlessly transitioning between the two control modes, the proposed approach guarantees the continued operation of the PMSM drive system even under sensor failure conditions. The feasibility of the algorithm is validated through MATLAB/Simulink simulation environment.

Keywords: *sensorless control, interior PMSM, permanent magnet synchronous motor, observer*

1. Introduction

Electric motors are widely recognized for their significant role across various sectors, including industrial automation, electric vehicles, and advanced machinery. The growing demand for electric motor applications, particularly in the shift from diminishing fossil fuels to electrical energy, has led to an increased focus on research and development in motor control systems [1]. Among all types of AC electric motors, interior permanent magnet synchronous motors (IPMSM) are getting more attention because of their characteristics and high torque density, and the price per unit is decreasing due to improved electric machine manufacturing technology. To control IPMSM, the most popular algorithm used to control the speed of AC electric motors is the rotor field-oriented control (FOC) strategy. The condition for implementing the FOC algorithm is having information about the rotor position, which is determined by the direct axis of the rotor. Fortunately, the angle of the rotating coordinate of PMSM is synchronous with the rotation of the magnetic flux. Rotor position information can be obtained by using an absolute encoder or a resolver.

The motors of electrical vehicles (EVs) are used at a wide range of speeds. The EVs can be used on highways with high-speed operation. Due to safety reasons, the seamless transition mode should be embedded into the control strategies of the EVs. In [2], the seamless transition of the PMSM compressor is presented. Based on the back electromotive force (EMF) and FOC strategy, the quick and seamless transition of PMSM was presented in [3]. The transition of full-speed regions with minimum voltage vector injection and EMF was presented in [4]. The sensorless for electrical vehicles was presented in [5-6]. Based on the regions of speed, different control algorithms will be adapted: control in low, medium, or high-speed regions. In low-speed regions, high-frequency voltage signal injection is frequently used, like high-frequency pulse voltage injection with random pulse sequence [2], square-wave voltage injection [3], and rotating high-frequency voltage injection [4]. For the safety of the drivers, the electrical angle can be used in two modes sensor and sensorless. Therefore, the fault of sensor needs to be detected to decide which mode should be used. The seamless transition from sensor to sensorless mode was presented in [8] for electric vehicles. This paper presents the transition of these two modes with a fault detection method. The originality of this paper is that the state observer for currents and electromotive forces on α and β axes can be obtained by using the poles' placement method.

The paper has five sections including an introduction, the mathematical model of IPMSM, Fault determination in the steady state algorithm, an illustrative example, and a conclusion.

2. Mathematical Models of IPMSM

This section provides two subsections consisting of the mathematical model of IPMSM and the state observer.

a. Mathematical model of Interior PMSM

Through mathematical transformations [9], we have

$$\begin{bmatrix} v_d \\ v_q \end{bmatrix} = \begin{bmatrix} R + pL_d & -\omega_{re} L_q \\ \omega_{re} L_q & R + pL_d \end{bmatrix} \begin{bmatrix} i_d \\ i_q \end{bmatrix} + \begin{bmatrix} 0 \\ (L_d - L_q)(\omega_{re} i_d - \dot{i}_q) + \omega_{re} K_E \end{bmatrix} \quad (1)$$

By using the Park transform yields

Received: 19 September 2024; Accepted: 15 November 2024.

$$\begin{bmatrix} v_\alpha \\ v_\beta \end{bmatrix} = \begin{bmatrix} R + pL_d & \omega_{re}(L_d - L_q) \\ -\omega_{re}(L_d - L_q) & R + pL_d \end{bmatrix} \begin{bmatrix} i_\alpha \\ i_\beta \end{bmatrix} + \left\{ (L_d - L_q)(\omega_{re} i_d - \dot{i}_q) + \omega_{re} K_E \right\} \begin{bmatrix} -\sin\theta_{re} \\ \cos\theta_{re} \end{bmatrix} \quad (2)$$

Consider the rear component in Eq. (2) as the electromotive force generated by the motor, we have

$$e = \begin{bmatrix} e_\alpha \\ e_\beta \end{bmatrix} = \left\{ (L_d - L_q)(\omega_{re} i_d - \dot{i}_q) + \omega_{re} K_E \right\} \begin{bmatrix} -\sin\theta_{re} \\ \cos\theta_{re} \end{bmatrix} = E \begin{bmatrix} -\sin\theta_{re} \\ \cos\theta_{re} \end{bmatrix} \quad (3)$$

By converting (2) to the state space model we have

$$p \begin{bmatrix} i_\alpha \\ i_\beta \end{bmatrix} = \frac{1}{L_d} \left\{ \begin{bmatrix} v_\alpha \\ v_\beta \end{bmatrix} - \begin{bmatrix} R_s & \omega_{re}(L_d - L_q) \\ -\omega_{re}(L_d - L_q) & R_s \end{bmatrix} \begin{bmatrix} i_\alpha \\ i_\beta \end{bmatrix} - \begin{bmatrix} e_\alpha \\ e_\beta \end{bmatrix} \right\} \quad (4)$$

Similarly, (3) can be written by

$$p \begin{bmatrix} e_\alpha \\ e_\beta \end{bmatrix} = p \left\{ (L_d - L_q)(\omega_{re} i_d - \dot{i}_q) + \omega_{re} K_E \right\} \begin{bmatrix} -\sin\theta_{re} \\ \cos\theta_{re} \end{bmatrix} = \begin{bmatrix} -\omega_{re} e_\beta \\ \omega_{re} e_\alpha \end{bmatrix} + \left\{ (L_d - L_q)(\omega_{re} \dot{i}_d - \ddot{i}_q) \right\} \begin{bmatrix} -\sin\theta_{re} \\ \cos\theta_{re} \end{bmatrix} \quad (5)$$

Combine the result of (4) and (5), the IPMSM state space model yield:

$$p \begin{bmatrix} i_\alpha \\ i_\beta \\ e_\alpha \\ e_\beta \end{bmatrix} = \begin{bmatrix} \frac{-R_s}{L_d} & -\omega_{re}\frac{L_d - L_q}{L_d} & \frac{-1}{L_d} & 0 \\ \omega_{re}\frac{L_d - L_q}{L_d} & \frac{-R_s}{L_d} & 0 & \frac{-1}{L_d} \\ 0 & 0 & 0 & -\omega_{re} \\ 0 & 0 & \omega_{re} & 0 \end{bmatrix} \begin{bmatrix} i_\alpha \\ i_\beta \\ e_\alpha \\ e_\beta \end{bmatrix} + \begin{bmatrix} \frac{1}{L_d} & 0 \\ 0 & \frac{1}{L_d} \\ 0 & 0 \\ 0 & 0 \end{bmatrix} \begin{bmatrix} v_\alpha \\ v_\beta \end{bmatrix} + \begin{bmatrix} 0 \\ 0 \\ -(L_d - L_q)(\omega_{re}\dot{i}_d - \ddot{i}_q)\sin\theta_{re} \\ (L_d - L_q)(\omega_{re}\dot{i}_d - \ddot{i}_q)\cos\theta_{re} \end{bmatrix} \quad (6)$$

Providing symbols to the matrices, the IPMSM state model becomes

$$\dot{\boldsymbol{X}} = \boldsymbol{AX} + \boldsymbol{BU} + \boldsymbol{W} \quad (7)$$

b. State Observer

Back Electromotive Force (Back EMF) Observer

The state observer model we propose is as follows:

$$\dot{\hat{\boldsymbol{X}}} = \boldsymbol{A}\hat{\boldsymbol{X}} + \boldsymbol{BU} + \boldsymbol{W} + \boldsymbol{LC}(\boldsymbol{X} - \hat{\boldsymbol{X}}) \quad (8)$$

From (7) and (8), the error between the observed state and the actual state $\boldsymbol{\varepsilon}$ can be obtained as:

$$\dot{\boldsymbol{X}} - \dot{\hat{\boldsymbol{X}}} = \boldsymbol{A}(\boldsymbol{X} - \hat{\boldsymbol{X}}) - \boldsymbol{LC}(\boldsymbol{X} - \hat{\boldsymbol{X}}) \quad (9)$$

or

$$\dot{\boldsymbol{\varepsilon}} = (\boldsymbol{A} - \boldsymbol{LC})\boldsymbol{\varepsilon} \quad (10)$$

where $\boldsymbol{\varepsilon} = \boldsymbol{X} - \hat{\boldsymbol{X}}$. Eq. (9) is asymptotically stable if there existed the positive matrices $\boldsymbol{P}$ and $\boldsymbol{Q}$ with

$$(\boldsymbol{A} - \boldsymbol{LC})^T \boldsymbol{P} + \boldsymbol{P}(\boldsymbol{A} - \boldsymbol{LC}) = -\boldsymbol{Q} \quad (11)$$

Proof: The Lyapunov can be selected by

$$\boldsymbol{V}(\boldsymbol{\varepsilon}) = \boldsymbol{\varepsilon}^T \boldsymbol{P} \boldsymbol{\varepsilon} \quad (12)$$

By taking the derivative of equation (12) yields

$$\begin{aligned} \dot{\boldsymbol{V}}(\boldsymbol{\varepsilon}) &= \dot{\boldsymbol{\varepsilon}}^T \boldsymbol{P}\boldsymbol{\varepsilon} + \boldsymbol{\varepsilon}^T \boldsymbol{P}\dot{\boldsymbol{\varepsilon}} \\ &= \boldsymbol{\varepsilon}^T (\boldsymbol{A} - \boldsymbol{LC})^T \boldsymbol{P}\boldsymbol{\varepsilon} + \boldsymbol{\varepsilon}^T \boldsymbol{P}(\boldsymbol{A} - \boldsymbol{LC})\boldsymbol{\varepsilon} \\ &= \boldsymbol{\varepsilon}^T \left((\boldsymbol{A} - \boldsymbol{LC})^T \boldsymbol{P} + \boldsymbol{P}(\boldsymbol{A} - \boldsymbol{LC}) \right) \boldsymbol{\varepsilon} \end{aligned} \quad (13)$$

since $(\boldsymbol{A} - \boldsymbol{LC})^T \boldsymbol{P} + \boldsymbol{P}(\boldsymbol{A} - \boldsymbol{LC}) < 0 \Rightarrow \dot{\boldsymbol{V}}(\boldsymbol{\varepsilon}) < 0$

c. Rotor angle estimation

After observing the EMF, the phase-locked loop (PLL) structure is used to obtain the rotor angle. The PLL structure is shown in Figure 1 below.

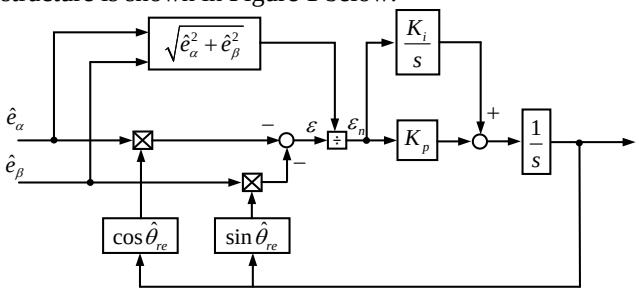

Fig. 1. Rotor angle tracking based on PLL.

The PLL stage lessens the difference between the estimated angle and the actual angle to zero. The above structure can be expressed mathematically as follows:

$$\begin{aligned} \varepsilon_n &= \frac{1}{\sqrt{\hat{e}_\alpha^2 + \hat{e}_\beta^2}} \left[-\hat{e}_\alpha \cos\hat{\theta}_{re} - \hat{e}_\beta \sin\hat{\theta}_{re} \right] \\ &= \frac{1}{E} \left[E\sin\theta_{re}\cos\hat{\theta}_{re} - E\cos\theta_{re}\sin\hat{\theta}_{re} \right] \\ &= \sin(\theta_{re} - \hat{\theta}_{re}) \approx \theta_{re} - \hat{\theta}_{re} \end{aligned} \quad (14)$$

3. Fault Determination In the Steady State Algorithm

a. Problem statement

In normal operating conditions, the speed and angle sensor signals will be given priority. However, in cases where external factors cause sensor or signal wire failures leading to significant errors, a switching algorithm will be used to maintain the operation of the drive system by recognizing and switching to the signals from the sensorless. The switching algorithm includes two parallel stages: calculating the error between the sensor and sensorless; and self-estimating the error.

b. The error between sensor and sensorless calculation

The sensorless observer is considered reliable in the steady state with a maximum angle error of θ_{err}. Based on this, when the angle error exceeds $2\theta_{err}$, the algorithm will issue a signal requesting to use the sensorless signal.

c. The error self-estimation

In the steady state, for each sample cycle, 10 previous speed values are collected to calculate root means square speed.

$$\omega_{rms} = \sqrt{\frac{1}{10}\sum_{i=1}^{10}\omega_{k-i}} \tag{15}$$

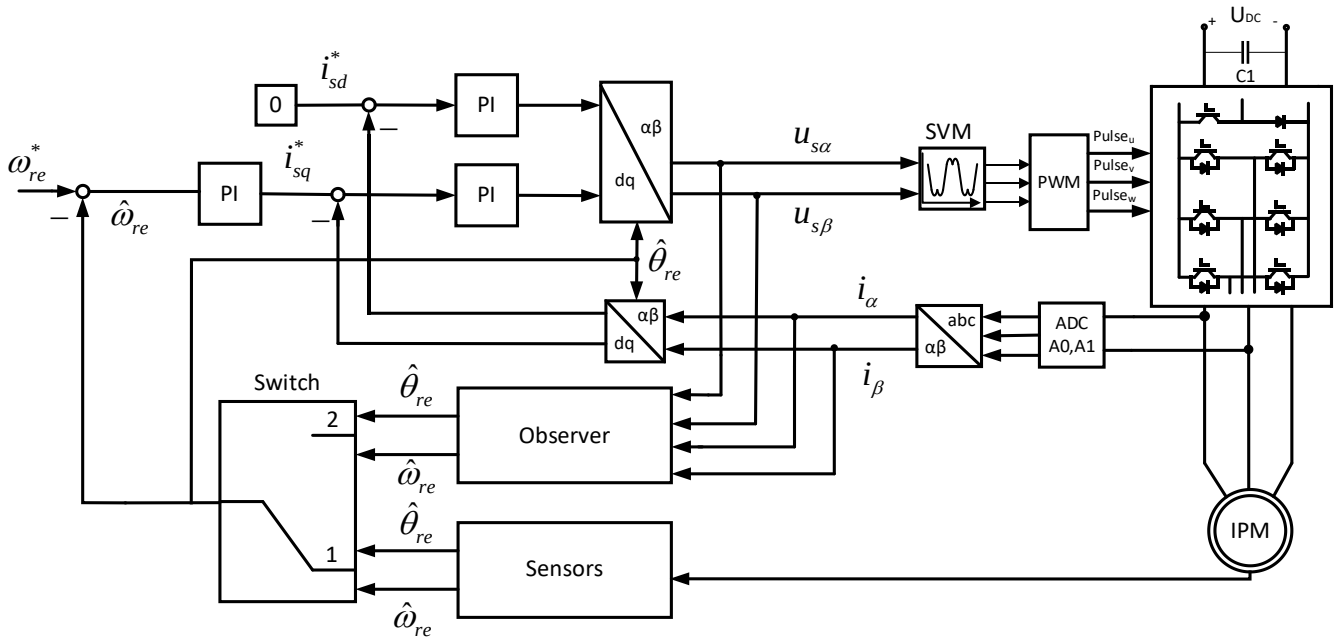

Fig. 2. FOC-based sensor to the sensorless control scheme.

If the error of the feedback speed signal and the RMS speed overshoots the peak error speed, which is the max error value of speed in 10 previous sample cycles, the algorithm will issue a signal requesting a change in the signal source.

When both two proposed stages require signal source transition, the switching algorithm will change to using the sensorless signal.

4. An Illustrative Example

The simulation system was built on MATLAB/Simulink. The main structure includes blocks related to the FOC control algorithm, state observer, and switching command. The actuator is a 3-phase inverter, switched on the principle of space vector modulation. The structure is shown in Fig. 2. The motor block used in the simulation is a synchronous motor with salient-pole classification, the motor parameters are shown in Table 1.

During the simulation, the α and β axis currents are taken directly from the transformation of sensors and then used to compare with the value from the observer. The EMF states of the α and β are observed so that the rotor angle can be obtained after using the PLL. The goal of this simulation is to evaluate whether the algorithm can operate stably at rated speed and load, checking the torque response, current response, and response of the state observer during the transition from the sensor signal to using the sensorless algorithm and vice versa, as well as whether the system operates stably. The motor will gradually accelerate from 0 to 2900 rpm. The sensor-based signal is used during this period. A scenario is considered when the system is in a steady state. Assume that a fault occurs, such as a wire tear, causing the sensor-based feedback signal to be lost. In this case, the switching algorithm will detect the issue and switch to using the sensorless feedback signal after 2 sampling cycles.

Table 1. Simulation parameters

Parameters	Symbol	Value	Unit
Rated power	P_{rated}	13	kW
Pole pairs	p	3	
Rated current	I_{rated}	58	A
Rated speed	ω_{rated}	2900	rpm
Rated torque	T_{rated}	42	Nm
Input voltage	V_{rated}	102	V
d axis inductance	L_d	0.9209	mH
q axis inductance	L_q	1.787	mH
Stator resistance	R_s	0.0025	Ω
Rotor magnetic flux	Ψ_r	0.109	Wb

Herein, at 9 (s), the feedback signal from the sensor was interrupted. The switching algorithm detected faults. Therefore, the transition from sensor mode to sensorless ode is executed with a time delay of 2e-5 (s). The

performance of the observer and the switching algorithm, as presented, are shown in Figures 3 to 6.

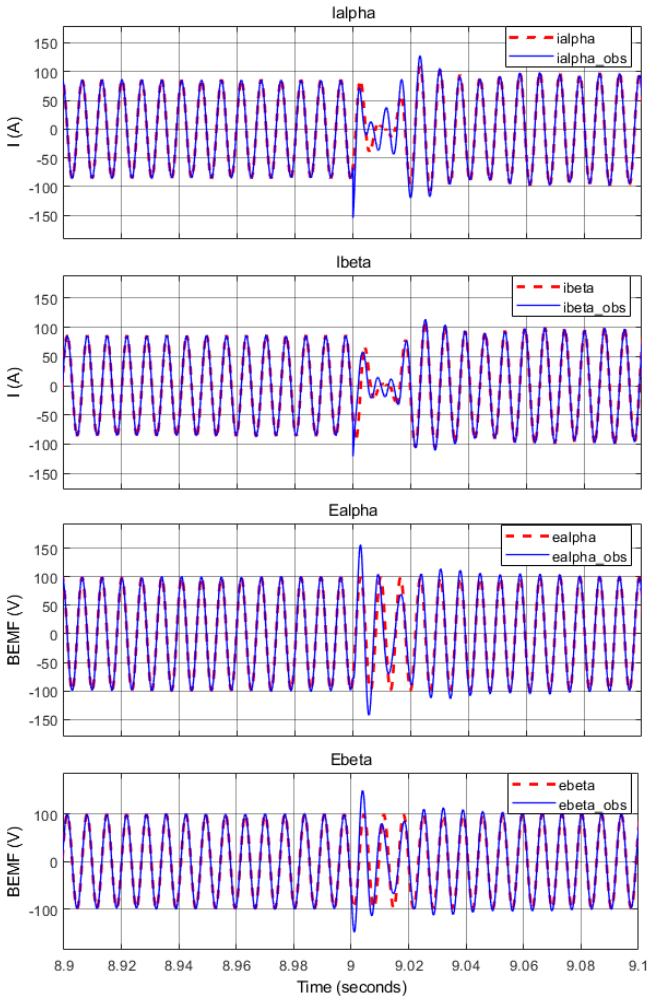

Fig. 3. Result of observer states at the switching point

In Figure 3, the back electromotive forces and currents are distorted at the transited time. After a short time, these estimated signals converged to real signals. The rotor angle in the transition time is shown in Figures 4-5. As shown in Figure 4, the estimated angle converged to the real angle in about 0.5 (s) and the maximum error was 7.6 degrees.

The torque is varied around the desired point as Figure 5. A significant electromagnetic torque fluctuation occurs during the switching process. After 0.1 (s), the torque converges to the load torque point.

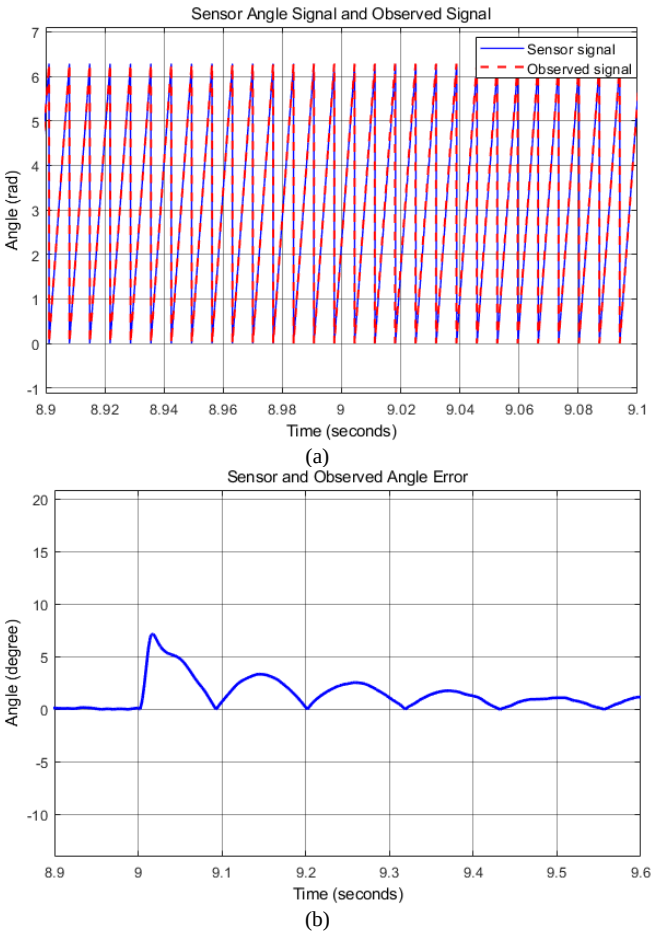

Fig. 4. Estimated and real rotor angle in the transmission time: (a) rotor angle signals in the transition time and (b) the error of estimated and real rotor angle around the transmission time.

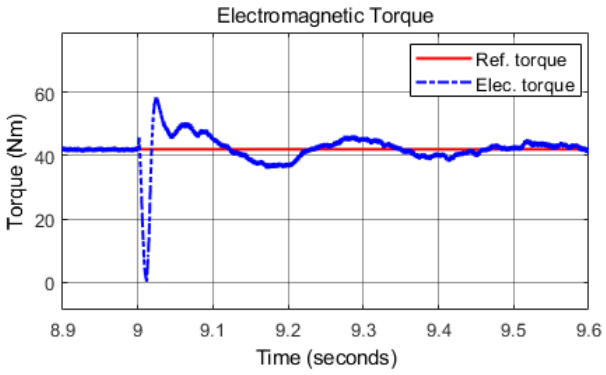

Fig. 5. Electromagnetic torque of sensorless and real torque load.

The performance of speed control based on the FOC with consideration of seamless switching time from sensor to sensorless mode is shown in Figure 6. The real speed of the motor converges to the desired speed with ripple is approximately 5 rpm or 0.17%. At the transition time, a small vibration occurs.

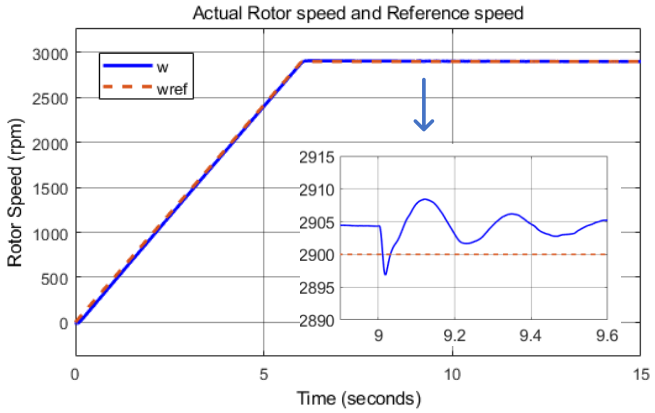

Fig. 6. Rotor speed signals

5. Conclusion

This paper presents the seamless transition by applying the state observer for back electromotive forces and stationary current axes. A fault determination method is proposed to detect sensor error. The control system's performance showed that the transmission between sensor mode to sensorless mode could be obtained with small torque vibration and speed around the transition point. Furthermore, the estimated signals were used to show that the designed observer is good in transmission mode. This is a suggestion for electric vehicle control systems.

Acknowledgment

This work was supported by the Ministry of Science & Technology, Vietnam, under Contract 01.M03.2023.

References

[1] B. K. Bose, "Power Electronics and Motor Drives Recent Progress and Perspective," *IEEE Transactions on Industrial Electronics*, vol. 56, no. 2, pp. 581 - 588, 2009.

[2] S. Chen, W. Ding, X. Wu, L. Huo, R. Hu and S. Shi, "Sensorless Control of IPMSM Drives Using High-Frequency Pulse Voltage Injection With Random Pulse Sequence for Audible Noise Reduction," *IEEE Transactions on Power Electronics*, vol. 38, no. 8, pp. 9395 - 9408, 2023.

[3] Z. Lin, X. Li, Z. Wang, T. Shi and C. Xia, "Minimization of Additional High-Frequency Torque Ripple for Square-Wave Voltage Injection IPMSM Sensorless Drives," *IEEE Transactions on Power Electronics*, vol. 35, no. 12, pp. 13345 - 13355, 2020.

[4] X. Wang, X. Fang, Z. Wang, Z. Zhong, Y. Wang, F. Lin and Z. Yang, "Self-adjusting strategy based on rotating injection for sensorless control of high-power PMSM drives," *ICPE 2019 - ECCE Asia*, 2019.

[5] J. Kang, *General Purpose Permanent Magnet Motor Drive without Speed and Position Sensor*, Yaskawa, 2009.

[6] S.-H. Kim, Electric Motor Control, Elsevier, 2017.

[7] Y. Li, H. Wu, X. Xu, X. Sun and J. Zhao, "Rotor Position Estimation Approaches for Sensorless Control of Permanent Magnet Traction Motor in Electric Vehicles: A Review," *MDPI*, vol. 12, 2021.

[8] N.-C. Park, Y.-K. Lee and S.-H. Kim, "Initial Rotor Position Estimation for an Interior Permanent-Magnet Synchronous Motor using Inductance Saturation," *KoreaScience*, vol. 16, no. 4, pp. 374-381, 2011.

[9] M. Sabra, B. Khasawneh and M. A. Zohdy, "Nonlinear Control of Interior PMSM Using Control Lyapunov Functions," *Journal of Power and Energy Engineering*, vol. 2, pp. 17-26, 2014.

[10] Z. Chen, M. Tomita, S. Doki and S. Okuma, "An Extended Electromotive Force Model for Sensorless Control of Interior Permanent-Magnet Synchronous Motors," *IEEE Transactions On Industrial Electronics*, vol. 50, no. 2, pp. 288-295, 2003.

[11] W. Yang, H. Guo, X. Sun, Y. Wang, S. Riaz and H. Zaman, "Wide-Speed-Range Sensorless Control of IPMSM," *Electronics*, vol. 11, no. 22, 2022.

[12] H. Jian and W. Song, "A sliding mode observer of IPMSM combining adaptive synchronous filter and back EMF estimator," *2020 7th International Forum on Electrical Engineering and Automation (IFEEA)*, 2020.

[13] and H.-Y. Wang, Ming-Shyan; Hsieh, Min-Fu; Lin, “electronics-07-00452-v2.pdf.” 2018. doi: https://doi.org/10.3390/electronics7120452.

[14] M. Cheng, L. Sun, G. Buja, and L. Song, “Advanced electrical machines and machine-based systems for electric and hybrid vehicles,” Energies, vol. 8, no. 9. pp. 9541–9564, 2015. doi: 10.3390/en8099541.

[15] “Speed sensorless control of permanent magnet synchronous motors using sliding-mode observer,” Journal of Science and Technology - HaUI, vol. 59, no. 2A. 2023. doi: 10.57001/huih5804.2023.048.